

Predicting gridded winter PM_{2.5} concentration in east of China

Zhicong Yin^{1,2,3*}, Mingkeng Duan¹, Yuyan Li¹, Tianbao Xu¹, Huijun Wang^{1,2,3}

¹Key Laboratory of Meteorological Disaster, Ministry of Education / Joint International Research Laboratory of Climate and Environment Change (ILCEC) / Collaborative Innovation Center on Forecast and Evaluation of Meteorological Disasters (CIC-FEMD), Nanjing University of Information Science & Technology, Nanjing, 210044, China

²Southern Marine Science and Engineering Guangdong Laboratory (Zhuhai), Zhuhai, 519080, China

³Nansen-Zhu International Research Centre, Institute of Atmospheric Physics, Chinese Academy of Sciences, Beijing, 100029, China

*Correspondence to: Zhicong Yin (yinzhc@nuist.edu.cn)

Abstract. Exposure to high levels of concentration of fine particle matters with diameter ≤ 2.5 μm (PM_{2.5}) can lead to great threats to human health in east of China. Air pollution control has greatly reduced the PM_{2.5} concentration and entered a crucial stage that required supports like fine seasonal prediction. In this study, we analysed the contributions of emission predictors and climate variability to seasonal prediction of PM_{2.5} concentration. The socioeconomic-PM_{2.5}, isolated by atmospheric chemical models, could well describe the gradual increasing trend of PM_{2.5} during the winters of 2001–2012 and the sharp decreasing trend since 2013. The preceding climate predictors have successfully simulated the interannual variability of winter PM_{2.5} concentration. Based on the year-to-year increment approach, a model for seasonal prediction of gridded winter PM_{2.5} concentration (10km \times 10km) in east of China was trained by integrating of emission and climate predictors. The area-averaged percentage of same sign was 81.4% (relative to the winters of 2001–2019) in the leave-one-out validation. In three densely populated and heavily polluted regions, the correlation coefficients were 0.93 (North China), 0.95 (Yangtze River Delta) and 0.87 (Pearl River Delta) during 2001–2019 and the root-mean-square errors were 6.8, 4.2 and 4.7 $\mu\text{g}/\text{m}^3$. More important, the significant decrease in PM_{2.5} concentration, resulted from implementation of strict emission control measures in recent years, was also reproduced. In the recycling independent tests, the prediction model developed in this study also maintained high accuracy and robustness. Furthermore, the accurate gridded PM_{2.5} prediction had the potential to support air pollution control on regional and city scales.

30 **1 Introduction**

31 Exposure to fine particle matters with diameter $\leq 2.5 \mu\text{m}$ ($\text{PM}_{2.5}$) can lead to severe respiratory and cardiovascular
32 diseases (Cohen et al., 2017) and even directly induces DNA damages (Wu et al., 2017). According to the newly
33 recommended air quality guidelines, the level of annual mean $\text{PM}_{2.5} > 5 \mu\text{g}/\text{m}^3$ has the potential to threat human health
34 (World Health Organization, 2021). In 2020, the average $\text{PM}_{2.5}$ concentration in cities of China was $33 \mu\text{g}/\text{m}^3$, although the
35 implementation of strict air quality control measures substantially reduced the emission of primary pollutants (Zhang et al.,
36 2022). The changes in the emission of air pollutants also resulted in the shift of winter $\text{PM}_{2.5}$ trend in east of China, that is,
37 the winter $\text{PM}_{2.5}$ concentration gradually increased during 2000–2012 but has been decreasing since 2013 (Figure 1a).
38 Evident interannual variation was also be found in the changes of $\text{PM}_{2.5}$ concentration in winter (December-January-
39 February), which was largely attributed to climate variability (Yin et al., 2020a, 2020b). Given the severe impact of $\text{PM}_{2.5}$
40 pollution and yearly plan of control action, it is meaningful and urgent to develop prediction models to forecast $\text{PM}_{2.5}$
41 concentration 1~3 months in advance. Furthermore, the predicting results should have high resolution to provide valuable
42 information on the regional and city levels.

43 To accurately predict climate anomalies is still a real challenge, while predicting air pollution on seasonal scale is much
44 harder than predicting routine meteorological elements (Wang et al., 2021). In general, the methods of climate prediction
45 included numerical climate models and statistical approaches. Despite the great advances in atmospheric chemical models in
46 recent years, most of these models were not designed for real-time operation of seasonal predictions and lacked the coupling
47 of the atmospheric chemical composition and the entire earth system (An et al., 2018). Additionally, statistical prediction of
48 winter $\text{PM}_{2.5}$ concentration was limited by the short sequences of observed atmospheric composition, because broad
49 observations only started in 2014 in China. The gray prediction model performed well in dealing with small sample data and
50 thus was used to forecast $\text{PM}_{2.5}$ concentration (Wang and Du, 2021; Wu et al., 2019; Xiong et al., 2019). Considering the
51 strong control measures implemented to improve air quality, the buffer operators can be added to the discrete gray prediction
52 model to reduce deviations (Dun et al., 2020). These mathematical models showed certain predictive skills, but lacked of
53 underlying physical mechanisms and long-standing robustness.

54 Many previous studies employed the long-term observed visibility, air humidity and weather phenomena to reconstruct
55 data of haze (Xu et al., 2016; Zou et al., 2017; He et al., 2019; Yin et al., 2020b). The change in winter haze days consists of
56 long-term trend and interannual-decadal variations. The long-term trend of haze was mainly determined by human activities
57 (i.e., primary pollutants emission and climate change), while its interannual-decadal variations had close relationships with
58 climate variability (Yin et al., 2020b; Geng et al., 2021a). Besides analysis of climate mechanisms, the number of haze days
59 was also used as a proxy-predictand of $\text{PM}_{2.5}$ pollution. Taking advantage of the memory effect in slow-varying climate
60 forcings (e.g., sea surface temperature and sea ice), the number of haze days was successfully predicted in North China (Yin
61 and Wang 2016; Yin et al., 2017), Yangtze River Delta (Dong et al., 2021) and Fenwei Plain (Zhao et al., 2021). Chang et al.
62 (2021) used regional stratospheric warming over northeastern Asia in November to predict haze pollution in the Sichuan

63 Basin in 5–7 weeks. Information from the preceding autumn El Niño was also extracted to predict winter haze days in South
64 China (Cheng et al., 2019) and aerosol optical depth over northern India (Gao et al., 2019). In most of these studies, the
65 predictand is area-averaged number of haze days, which was a bit different from PM_{2.5} concentration in use and fine spatial
66 information was missing.

67 The Tracking Air Pollution (TAP) database combines information from ground observations, satellite retrievals,
68 emission inventories and chemical transport model simulations based on data fusion. A full-coverage PM_{2.5} reanalysis
69 dataset with a spatial resolution of 10km×10km from 2000 until present has been released (Geng et al., 2021b). It becomes
70 feasible to develop statistical prediction model of PM_{2.5} concentration based on this long-range dataset. Furthermore, as
71 reviewed by Yin et al., (2022), the predictability of winter haze decreased after 2014, which was mainly attributed to the
72 disturbances from super-strict emissions reduction in China. Rapid changes in human activities and changes in climate
73 anomalies both should be considered and included in PM_{2.5} prediction models. This is the major motivation of the present
74 study to build a climate-emission hybrid model for the prediction of gridded PM_{2.5} concentration in east of China. The
75 findings of this study have enormous potentials to support fine designs and implements of air pollution control in advance.

76 **2 Datasets and method**

77 **2.1 Data**

78 The monthly sea ice concentration (SI) and sea surface temperature (SST) dataset from 2000 to 2019, with a spatial
79 resolution of 1°×1°, were provided by the Met Office Hadley Centre (Rayner et al. 2003,
80 <https://www.metoffice.gov.uk/hadobs/hadisst/>). Monthly soil moisture (Soilw), snow depth (SD), geopotential height at
81 500hPa (Z500) and 850hPa (Z850), sea level pressure (SLP) and 10m wind were extracted from the fifth generation
82 reanalysis product (ERA5) produced by the European Center for Medium Range Weather Forecasts (Hersbach et al. 2020,
83 <https://cds.climate.copernicus.eu/#!/search?text=ERA5&type=dataset>). Annual emissions of ammonia, nitrogen oxide, BOC,
84 primary PM_{2.5}, and sulfur dioxide in China were derived from the MEIC model (<http://www.meicmodel.org/>; Li et al., 2017).

85 Hourly site-observed PM_{2.5} concentration during 2014–2019 were also employed in the present study
86 (<https://www.aqistudy.cn/historydata/>). The long-term and high-resolution TAP PM_{2.5} concentration dataset during 2000-
87 2019 can be downloaded from <http://tapdata.org> (Geng et al. 2021b). The PM_{2.5} reanalysis data were used as training data as
88 well as test data in the construction of the prediction model, and the observed PM_{2.5} concentration were also applied to verify
89 the prediction skill of the model.

90 **2.2 Isolation of socioeconomic-PM_{2.5}**

91 We employed the simulated annual-mean PM_{2.5} concentrations that exclude the meteorological contributions to
92 represent the impacts of anthropogenic emissions. Compared with direct use of emission inventory of primary pollutants, the

93 isolated socioeconomic-PM_{2.5} (SE-PM_{2.5}) involved both results of emission changes and follow-up physical and chemical
94 reactions in the air. To remove the meteorological influences from the TAP PM_{2.5} data, we used chemical transport models
95 and emission inventories to separate the contributions from emission and meteorology changes. Following the approach
96 proposed by Xiao et al. (2021), we used a ‘fix emission’ scenario to quantify the impacts of interannual meteorological
97 variation on PM_{2.5} concentration in Community Multiscale Air Quality (CMAQ) model. Subsequently, a full simulation with
98 year-by-year emission and meteorology was completed. Differences between the ‘fix emission’ simulation and the full
99 simulation were considered to be PM_{2.5} concentrations driven by anthropogenic emissions. This data has been analyzed to
100 quantify relative influences of different drivers on PM_{2.5}-related deaths in China (Geng et al. 2021b).

101 2.3 Year-to-year increment prediction

102 The year-to-year increment approach is proposed to improve the skill of climate prediction (Wang et al., 2008), in
103 which the predicted object is not climate anomalies but is the difference between the current and the previous year (DY).
104 After adding the predicted DY to the observed predictand in the year before, the final predicted results during 2001–2019
105 were obtained. Based on full use of observations in the previous year, the gradually changing trend and inter-decadal
106 components can be well reproduced. Anthropogenic-natural-forcing predictand could be represented by $Y = YS + YC$, where
107 YS and YC denoted the slowly varying socio-economic and climatic components, respectively. In the DY approach, which
108 was expressed by:

$$109 \quad DY = Y_t - Y_{t-1} = (YS_t + YC_t) - (YS_{t-1} + YC_{t-1}) = (YS_t - YS_{t-1}) + (YC_t - YC_{t-1})$$

110 where the subscripts t and $t-1$ indicated the current and the previous years. Before 2013, the difference between
111 anthropogenic emissions in two adjacent years was small, Yin and Wang (2016) assumed $(YS_t - YS_{t-1}) \approx 0$ and proposed
112 that DY was mainly influenced by climate variability. However, due to significant reduction of anthropogenic emissions
113 after the implementation of China’s Air Pollution Prevention and Control Action Plan (Zhang and Geng, 2020), the
114 assumption of $(YS_t - YS_{t-1}) \approx 0$ was no longer completely valid. Therefore, it is meaningful to consider the information of
115 rapid emission changes and re-build the prediction model (Yin et al., 2022).

116 (1) Seasonal prediction model based on SE-PM_{2.5} (SP-SE): this prediction model unilaterally emphasized the impacts of
117 human activities and was trained by DY of SE-PM_{2.5} in each grid.

118 (2) Seasonal prediction model based on preceding climate variability (SP-CV): this prediction model was highly
119 focused on the impacts of climate condition and trained by DY of closely related climate factors.

120 (3) Seasonal prediction model based on both SE-PM_{2.5} and climate (SP-EC): the contributions of emissions and climate
121 factors are incorporated into one prediction model, i.e., combining the PM_{2.5} DY from SP-SE and SP-CV.

122 In the leave-one-out cross validation, root-mean-square error (RMSE), relative bias and correlation coefficient (CC)
123 were calculated. When discussing the CC after the detrending, the linear trend was removed by stages (i.e., winters of 2001-

124 2011 and 2012–2019). The percentage of the same sign (PSS; same sign means the mathematical sign of the fitted and
125 observed $PM_{2.5}$ anomalies was the same) was also computed.

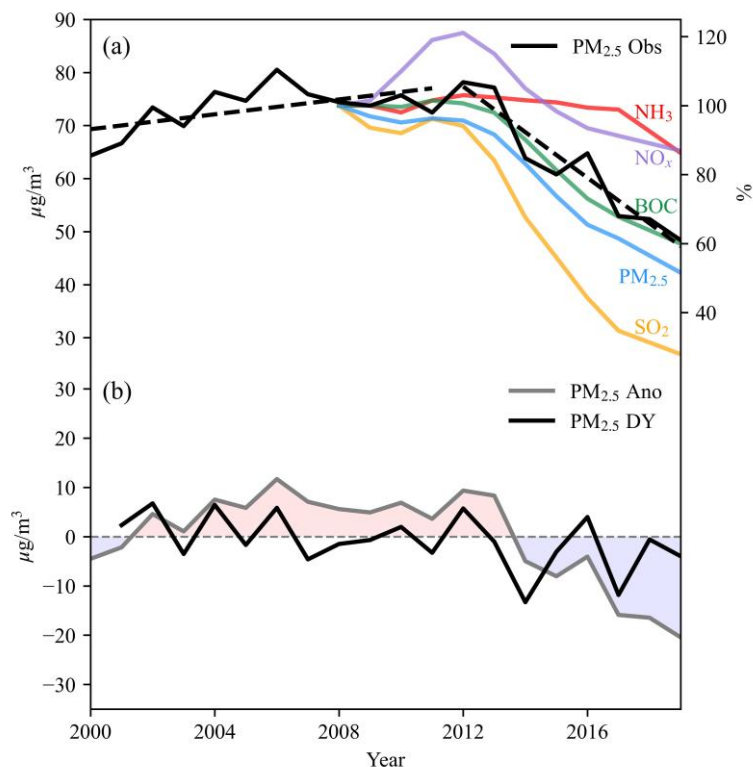
126 **3 Relative contributions of emission and climate predictors**

127 **3.1 Roles of emission**

128 Human activities are the major source of haze pollution in east of China (Zhang and Geng, 2020), which implies that a
129 large proportion of $PM_{2.5}$ concentration is predictable. Particularly, the large reduction of anthropogenic emissions since
130 2013 determined the decreasing trend of winter $PM_{2.5}$ concentration (Figure 1a). As aforementioned, the socioeconomic-
131 $PM_{2.5}$ (i.e., SE- $PM_{2.5}$) isolated by CMAQ could well reflect the impacts of human activities and was a potentially effective
132 predictor for seasonal prediction of $PM_{2.5}$ concentration. As expected, the one-variable linear regression model based on
133 anomalies of SE- $PM_{2.5}$ successfully reproduced different slopes of trend during 2001–2007, 2008–2013 and 2014–2019, but
134 the predicted $PM_{2.5}$ concentration varied too smoothly (Figure S1a). Furthermore, the quantities were underestimated when
135 observed $PM_{2.5}$ concentration increased and overestimated when $PM_{2.5}$ concentration rapidly decreased. To eliminate the
136 influence of trend shift, we calculated DY of $PM_{2.5}$ and SE- $PM_{2.5}$. Compared with its anomalies, $PM_{2.5}$ DY did not show
137 significant trend but displayed regularly oscillating characteristic (Figure 1b), and its predictability was much better (Wang
138 et al., 2008). The SP-SE model was trained by DY of SE- $PM_{2.5}$ in each grid to predict $PM_{2.5}$ DY. After adding the predicted
139 $PM_{2.5}$ DY to observed $PM_{2.5}$ in the previous year, the final $PM_{2.5}$ concentration was obtained. The CC between predicted and
140 observed $PM_{2.5}$ was 0.87 during 2001–2019 in the east of China. The underestimated (2001–2007) and overestimated (2014–
141 2019) values in Figure S1a were largely corrected and interannual variation also appeared in the results of SP-SE prediction
142 (Figure S1b). The staged trends from the SP-SE model almost overlapped with the observed trends, indicating the model
143 performed well in capturing the changes of trend (Figure S2).

144 North China (NC; 34–42°N, 114–120°E), the Yangtze River Delta (YRD; 27–34°N, 117–122°E) and the Pearl River
145 Delta (PRD; 21.5–25°N, 112–116°E) are three regions that have been experiencing severe $PM_{2.5}$ pollution (Yin et al., 2015).
146 Thus, the performance of the SP-SE model in NC, the YRD and the PRD were validated separately (Table 1, Figure 2 a-c).
147 The RMSEs were 12.2, 6.2 and 6.8 $\mu\text{g}/\text{m}^3$ in NC, the YRD and the PRD, respectively (Table 1). Larger RMSE in NC did not
148 indicate the SP-SE model performs worse in NC than in the YRD and the PRD, because the mean value of $PM_{2.5}$
149 concentration was the highest in NC. The relative bias (absolute bias/mean) in NC was 8.5%, which was smaller than that in
150 the PRD (12.9%). Consistent with its performance in east of China, the SP-SE model also well reproduced the staged trends
151 in NC, the YRD and the PRD (Figure 2 a-c). However, when the linear trend was removed, the CC between predicted and
152 observed $PM_{2.5}$ significantly decreases in all the three $PM_{2.5}$ -polluted regions (NC: from 0.78 to -0.13; YRD: from 0.88 to -
153 0.28; PRD: from 0.74 to 0.16). That is, the prediction model trained by the socioeconomic- $PM_{2.5}$ could well predict the

154 values and staged linear trends. However, it certainly had no ability to simulate the interannual variability of PM_{2.5}
 155 concentration.



156

157 **Figure 1: Variation in (a) winter PM_{2.5} concentration (black; unit: ug/m³), (b) PM_{2.5} anomalies (gray; compared to the mean of**
 158 **2000–2019; unit: ug/m³) and PM_{2.5} DY (black; unit: ug/m³). Color lines in panel (a) indicate relative variations in annual emissions**
 159 **(compared to that in 2008, unit: %) of ammonia (NH₃; red), nitrogen oxide (NO_x; purple), BOC (green), PM_{2.5} (blue), and sulfur**
 160 **dioxide (SO₂; yellow) in east of China. The black dashed line in panel (a) indicates the linear trend of PM_{2.5} concentration.**

161 **Table 1: The leave-one-out validated root-mean square errors (RMSE), relative biases (absolute bias mean; %) and percentages of**
 162 **same sign (PSS) for three statistical models.**

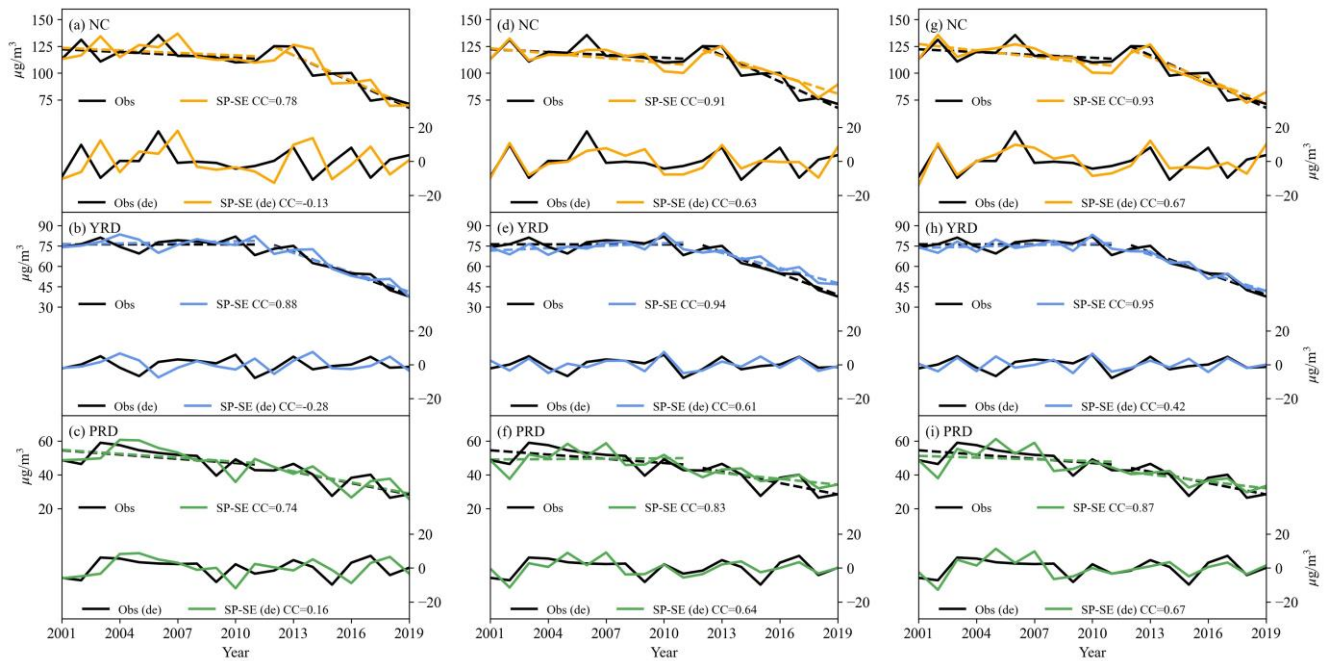
	RMSE (μg/m ³)			Relative Bias (%)		
	NC	YRD	PRD	NC	YRD	PRD
SP-SE	12.2	6.2	6.8	8.5	6.9	12.9
SP-CV	8.0	4.8	5.2	5.3	6.2	9.9
SP-EC	6.8	4.2	4.7	5.1	4.9	8.8

163

164

165

166



167

168

Figure 2: Variations in reanalysis (black) and SP-SE predicted winter PM_{2.5} concentration in (a) NC (orange), (b) the YRD (blue), and (c) the PRD (green) from 2001 to 2019 before (upper) and after (lower) detrending. The predicted PM_{2.5} is dependent on the leave-one-out validation. (d-f) are the same as (a-c), but for SP-CV. (g-i) are the same as (a-c), but for SP-EC.

169

170

171

3.2 Impacts of climate variability

172

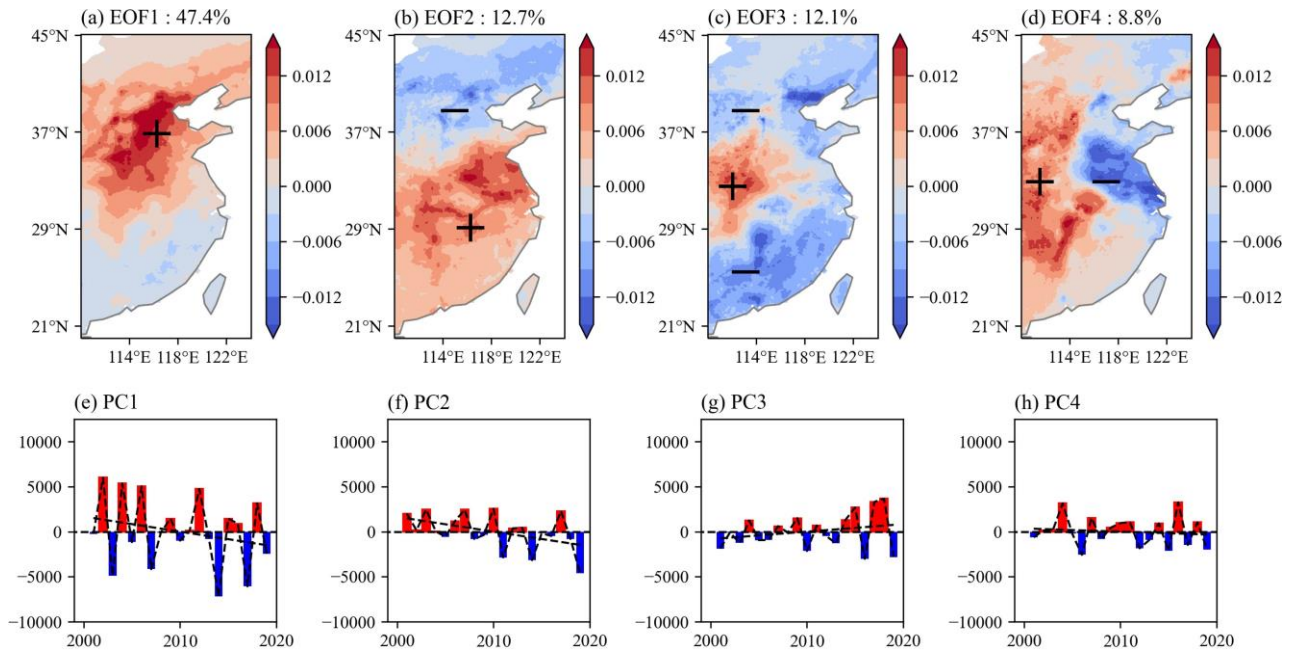
Decomposition and prediction of dominant modes of climate conditions were applied in short-term prediction of precipitation (Huang et al., 2022) and surface air temperature (Hsu et al., 2020) in east of China. In this study, we decompose the first four leading modes of PM_{2.5} DY during 2001-2019 (accumulated variance contribution=81%) produced by Empirical Orthogonal Function (EOF) analysis, built prediction model for each principal component respectively, recalculate the predicted PM_{2.5} DY by projecting the predicted PCs onto the observed EOF spatial patterns, and finally added the predicted PM_{2.5} DY to the observation in previous year to finish the development of SP-CV (Figure S3, Table S1). The interannual-decadal variation in haze pollution could be well explained by meteorological condition and preceding climate forcings (Yin et al., 2020b) such as the Arctic sea ice extent (Wang et al., 2015; Yin et al., 2019), Eurasia snow (Zou et al., 2017) and soil moisture (Yin and Wang 2018), SST in the Pacific (Yin and Wang 2016; He et al., 2019) and Atlantic (Yin and Zhang 2020a). Prediction signals from these climate anomalies could be observed before winter and owned specific physical implications.

183

The first EOF mode of PM_{2.5} DY illustrated heavily haze-polluted status in NC (Figure 3a, e). According to the correlation analysis, the September SST DY in the Southwest Pacific (CC with PC1=-0.73; Figure 4a) and October SST DY

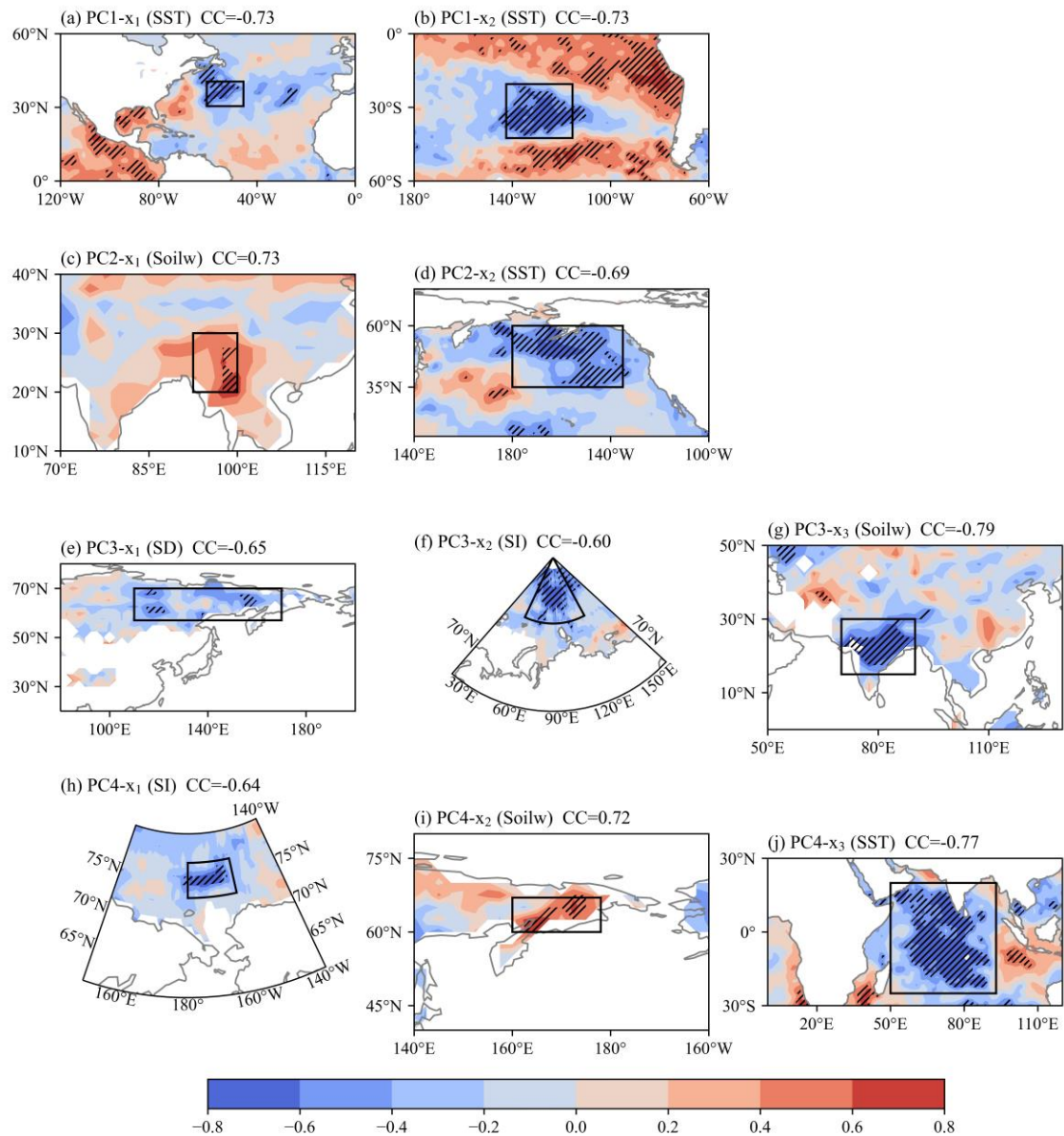
184

185 in the Sargasso Sea ($CC=-0.73$; Figure 4b) were selected to be the two predictors for PC1 of $PM_{2.5}$ DY (Table S1). Both of
 186 the predictors had close relationships with dipole pattern of Eurasian cyclonic and Northeast Asian anti-cyclonic circulations
 187 (Figure S4b, c), which was identical to those associated with PC1 (Figure S4a) and could restrain the invasion of cold air
 188 from high latitude into NC. The second EOF mode of $PM_{2.5}$ DY showed a ‘north-south’ dipole pattern (Figure 3b, f). The
 189 variations of $PM_{2.5}$ DY in Huanghuai and the YRD accounted for a large proportion. The October soil moisture DY in the
 190 Indo-China Peninsula (CC with PC2=0.73; Figure 4c) and June-August SST DY in the Gulf of Alaska ($CC=-0.69$; Figure 4d)
 191 were selected to build prediction model of PC2 (Table S1). The anomalous atmospheric circulation associated with PC2 and
 192 its predictors could enhance cold air invasion to NC (strong northerlies) but prevented the cold air from moving further south
 193 (weak 10m winds in Figure S4 d-f).



194

195 **Figure 3: Spatial patterns (a–d) and corresponding PCs (e–h) of the first four EOF modes for winter $PM_{2.5}$ DY in east of China**
 196 **during 2000–2019. The variance accounted for by each EOF mode is given in the panel.**



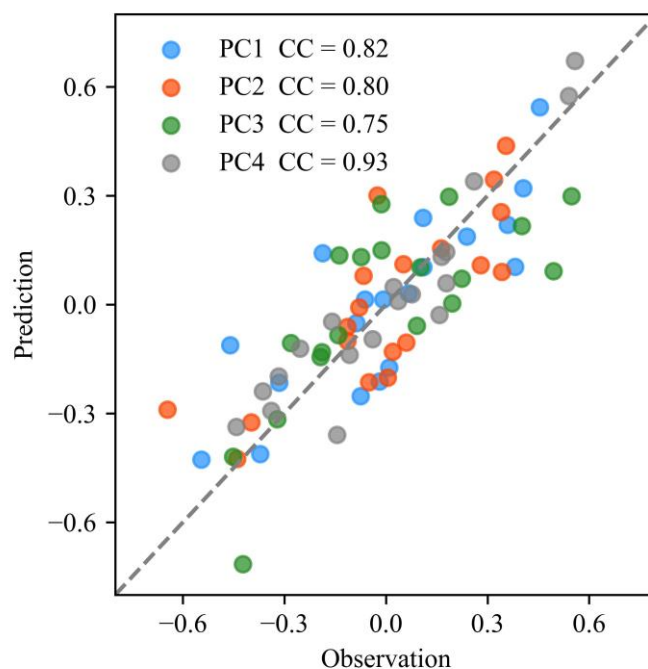
197

198 **Figure 4: CCs between climate predictors and (a-b) PC1, (c-d) PC2, (e-g) PC3, (h-j) PC4 from 2000 to 2019. The predictors for**
 199 **PC1 are (a) September SST over the South Pacific Ocean and (b) October SST over the Sargasso Sea. The predictors for PC2 are**
 200 **(c) October Soilw over the Indo-China Peninsula and (d) June-August SST over the Gulf of Alaska. The predictors for PC3 are (e)**
 201 **October Sd over eastern Siberia, (f) October SI over the Kara Sea and (g) September-October Soilw over the Indian Peninsula.**
 202 **The predictors for PC4 are (h) October SI over the Chukchi Sea, (i) October soil moisture over the Kamchatka Peninsula and (j)**
 203 **August-September SST over the Arabian Sea and the Bay of Bengal. The slashes indicate CCs exceeding the 95% confidence level.**
 204 **The black boxes indicate the regions over which the predictors are calculated.**

205 The third EOF mode indicated a triple pattern with centers located in the east of Inner Mongolia, the Fenwei Plain and
206 South China, respectively (Figure 3c, g). The Fenwei Plain was highly polluted and gained a great attention in recent years,
207 while the other two centers have relatively better air quality (Zhao et al., 2021). The October snow depth DY in eastern
208 Siberia (CC with PC3=-0.65; Figure 4e), October sea ice DY in the north to Barents Sea (CC=-0.60; Figure 4f) and
209 September-October soil moisture DY in the Indian Peninsula (CC=-0.79; Figure 4g) were considered in the prediction
210 model (Table S1). The predictors possibly induced atmospheric responses in winter (Figure S4 h-j) that were similar to PC3
211 (Figure S4 g). The abnormal northerlies over North China and South China enhanced the horizontal dispersion of haze
212 particles (Zhong et al., 2019), while the weak wind speed and surface wind convergence in central China were conducive to
213 the accumulation of pollutants. A statistical model (Table S1) was also developed to predict the ‘East-West’ dipole shown in
214 the fourth EOF mode (Figure 3d, h) based on October sea ice DY in the Chukchi Sea (CC=-0.64; Figure 4h), October soil
215 moisture DY in the Kamchatka peninsula (CC=0.72; Figure 4i) and August-September SST DY in the Arabian Sea
216 (CC=-0.77; Figure 4j). The atmospheric anomalies in the lower troposphere and near surface, which were associated with
217 the above predictors and PC4, also had similar impacts on haze pollution (Figure S4 k-n).

218 As shown in Figure 5, multiple linear regression model demonstrated good performance in simulating the variation in
219 each PC. The CCs between observed and predicted 1st-4th PCs were 0.82, 0.80, 0.75 and 0.93, respectively, all of which
220 were above the 99% confidence level, indicating that the model successfully reproduced each individual EOF mode.
221 Meanwhile, the yearly increment approach had the ability to address trend and its changes that were not obviously
222 mutational (Yin and Wang 2016). The CC between observed and predicted PM_{2.5} concentrations before (after) detrending by
223 stages was 0.91 (0.63) in NC, 0.94 (0.61) in the YRD and 0.83 (0.64) in the PRD in the leave-one out validation (Figure 2 d-
224 f). Thus, the SP-CV model well simulated both the trend and the interannual variation of PM_{2.5} concentration in the east of
225 China. In addition, the RMSEs in NC, the YRD and the PRD were 8.0, 4.8 and 5.2 μg/m³ and the relative biases were 5.3%,
226 6.2% and 9.9%, respectively (Table 1), all of which were obviously smaller than those of SP-SE. The PSS, which is an
227 important indicator of climate prediction, was also evaluated relative to the winters of 2001–2019. The area-averaged PSS
228 from SP-CV was 79.9% in east of China, which was 7.9% higher than that from SP-SE (Figure 6). Although the SP-CV
229 model performed better than the SP-SE, especially that it could capture the sharp downward trend after 2013 in NC and
230 YRD, the RMSEs of the SP-CV simulations for the period 2015-2019 increased up to 11.6, 6.5 and 5.3 μg/m³ in NC, the
231 YRD and the PRD compared to that of the SP-SE simulations. Obvious positive biases were found in the predictions of
232 PM_{2.5} concentration after 2014 (Figure 2 d-f) because the SP-CV model was short of information about the super-strict
233 emission regulations (Figure S2). Based on different levels of haze pollution, various degrees of air pollution control were
234 carried out in NC, the YRD and the PRD (Zhang and Geng, 2020). In NC, where anthropogenic emissions were most
235 prominently restricted, the predicted biases were also the largest (Figure 2d). The predicted biases were the smallest in the
236 PRD, while that in the YRD were in-between. These results were consistent with different intensities of pollution control in

237 the three regions (Figure 2e, f), which further indicated the importance to fully take into account the impacts of climate
238 variability and anthropogenic emissions.



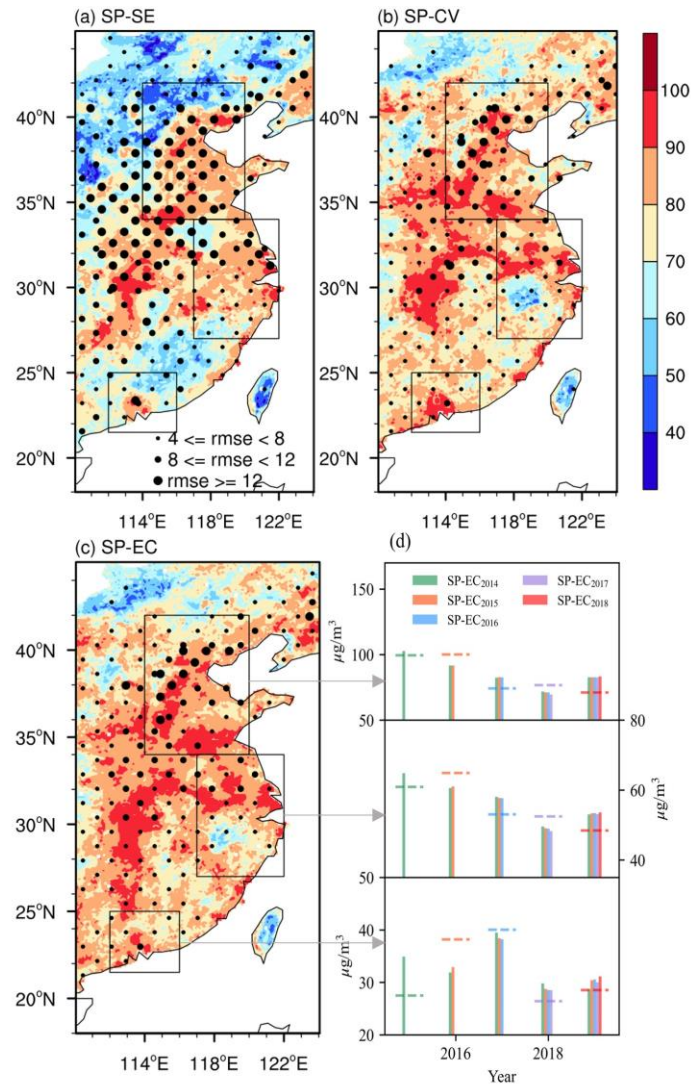
239
240 **Figure 5: Scatter plots of normalized observed (x axis) and predicted (y axis) PC1 (blue), PC2 (red), PC3 (green) and PC4 (gray)**
241 **from 2000 to 2019. The predicted PCs are dependent on the leave-one-cross validation.**

242 **4 PM_{2.5} prediction with integrated factors**

243 As aforementioned, the SP-SE model trained by the SE-PM_{2.5} DY considered the impacts of emission changes one-
244 sidedly and could well simulate the values and staged trends. However, it completely failed to reproduce the interannual
245 variation of winter PM_{2.5} concentration in east of China (Figure 2 a-c). Differently, the predictors of climate variability could
246 introduce the interannual variation of winter PM_{2.5} and the yearly increment approach had the ability to bring in the slow
247 trend. The SP-CV model successfully predicted most of the trend and interannual variation in PM_{2.5} concentration (Figure 2
248 d-f) but underestimated the sharp decreasing trend (Figure S2), which led to positive forecast biases after 2013 (Figure 2d-f).

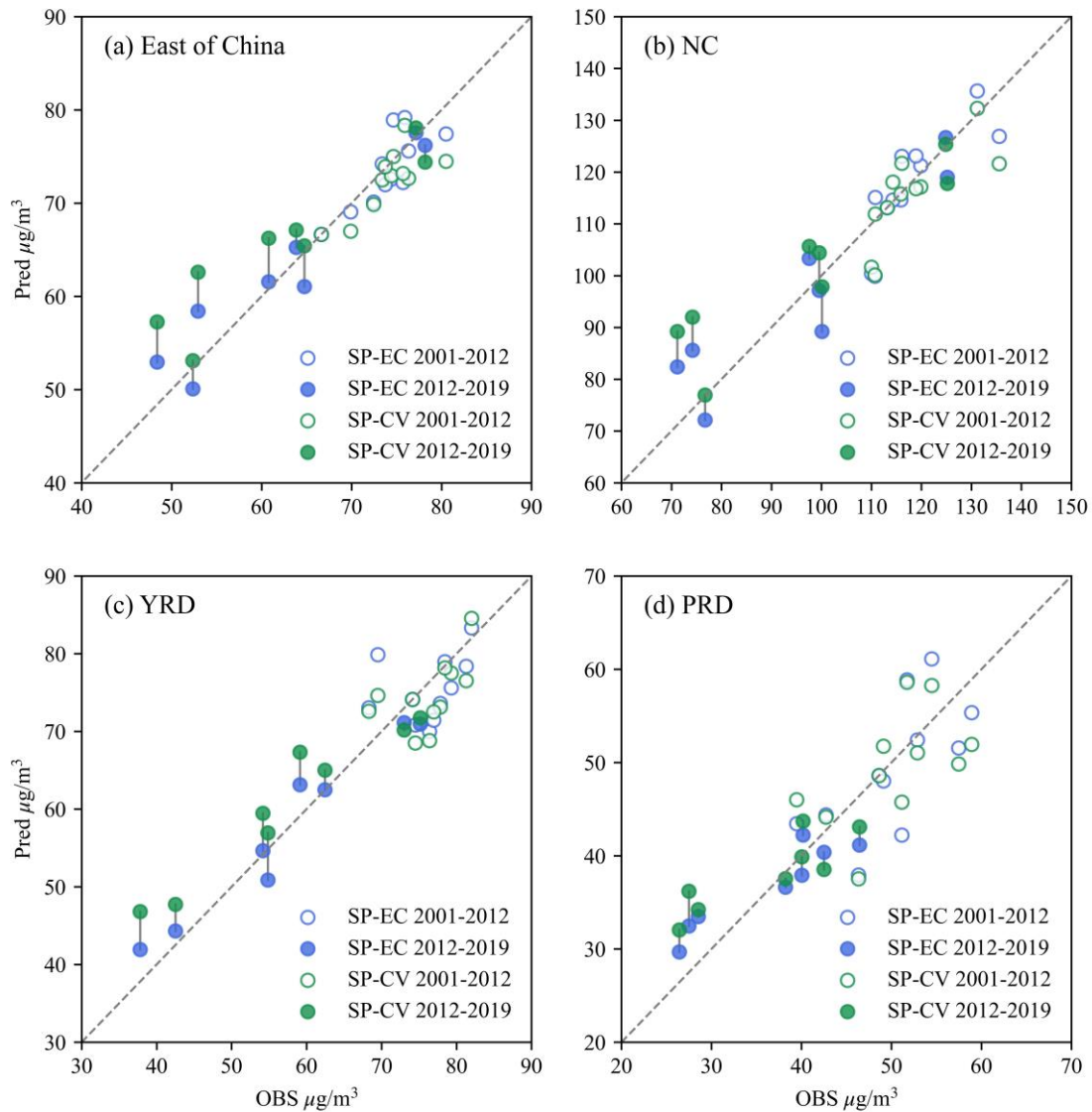
249 To fully contain predictive signals of human activities and climate anomalies, the predicted PM_{2.5} DY from SP-SE and
250 SP-CV model for the current year were added up and the sum was added to PM_{2.5} observations in the previous year to
251 develop the final prediction model, i.e., the SP-EC model. As expected, the performance of SP-EC model was better than
252 that of both SP-SE and SP-CV models. Area-averaged PSS was 81.4% in east of China (Figure 6). The CC between
253 observed and SP-EC-predicted PM_{2.5} concentrations before (after) detrending was 0.96 (0.74) in east of China; the RMSE

254 was $2.7 \mu\text{g}/\text{m}^3$, which was 43.8% (32.5%) smaller than the RMSE of SP-SE (SP-CV) in the leave-one out validation. That is,
255 the trend simulated by the SP-EC model almost overlapped with the trend of observations (similar to results of SP-SE) and
256 the interannual variation was also reproduced (similar to results of SP-CV). The CCs between observed and SP-EC-predicted
257 $\text{PM}_{2.5}$ concentrations before (after) detrending were 0.93 (0.67) in NC, 0.95 (0.42) in the YRD and 0.87 (0.67) in the PRD
258 (Figure 2g-i). The RMSEs were 6.8 in NC, 4.2 in YRD and $4.7 \mu\text{g}/\text{m}^3$ in PRD, which were 44.3% (15.0%), 32.3% (12.5%)
259 and 30.9% (9.6%) smaller than that of SP-SE (SP-CV), indicating greater improvements in NC than in the other two regions
260 (Table 1). According to the relative biases, the SP-EC model also demonstrated a better skill in NC (5.1%) than that in the
261 YRD (4.9%) and the PRD (8.8%) in the leave-one out validation. As shown in Figure 7, the decreases in $\text{PM}_{2.5}$ resulted from
262 the implementation of strict emission control measures in recent years were also reproduced by the SP-EC model. The
263 evident and positive biases in the SP-CV results were largely corrected in east of China, NC, the YRD and the PRD (Figure
264 7).



265

266 **Figure 6: Distributions of PSS (shadings) and RMSE (dots) from (a) SP-SE, (b) SP-CV, and (c) SP-EC. The boxes represent NC,**
 267 **the YRD and the PRD respectively, and the arrows point to the SP-EC predicted $\text{PM}_{2.5}$ in recycling independent tests (bars) and**
 268 **observations (dashed lines) corresponding to the area. The subscript in the legend of panel (d) indicates the model trained from**
 269 **2000 to this year, and the $\text{PM}_{2.5}$ from the next year to 2019 are independently predicted.**

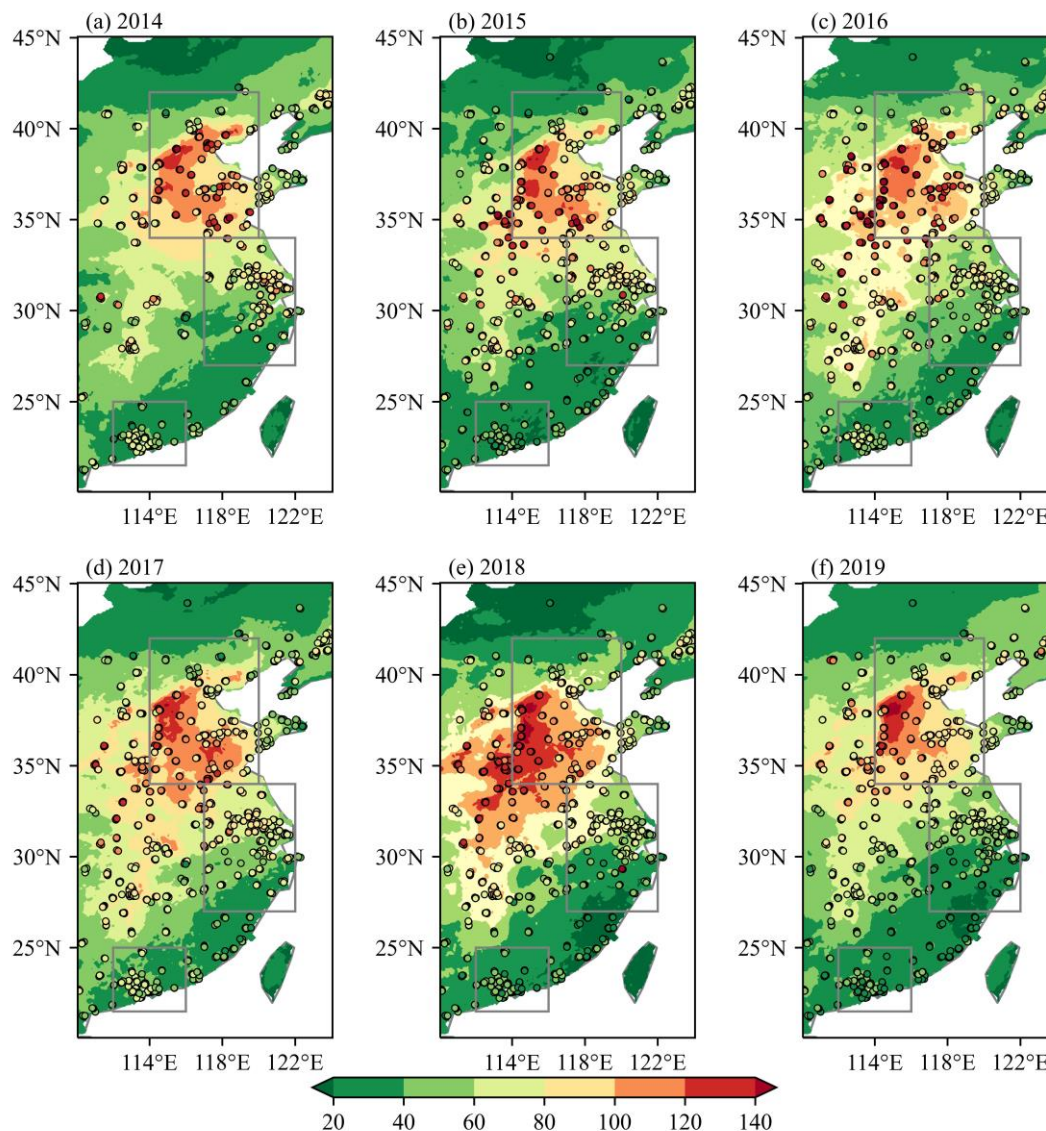


270

271 **Figure 7: Scatter plots of the reanalysis (x axis) and predictions of (y axis) $PM_{2.5}$ concentration by SP-CV (green) and SP-EC (blue)**
 272 **in (a) east of China, (b) NC, (c) the YRD and (d) the PRD. The points during 2012–2019 are filled and the short lines between SP-**
 273 **CV and SP-EC points indicate the calibrations.**

274 High spatial resolution was one of the advantages of the seasonal prediction model developed in this study. That is, the
 275 SP-EC model could predict winter $PM_{2.5}$ concentration at each $10km \times 10km$ grid in east of China. When only considering
 276 emission predictors (i.e., SP-SE), $RMSEs > 12 \mu g/m^3$ were found in middle part of the study region and the PSS was lower
 277 than 60% in South China and the Inner Mongolia (Figure 6a). When only considering climate predictors (i.e., SP-CV),
 278 $RMSEs > 12 \mu g/m^3$ existed in Beijing and its surrounding areas and PSS significantly increased compared to the result of SP-

279 SE (Figure 6b). When integrating both of the emission predictors and climate predictors (i.e., SP-EC), the RMSE in each
280 grid further decreased and the PSS also increased (Figure 6c). In middle part of the study region, the PSS was higher than
281 80%. In view of gaps between site observations and model simulations, the SP-EC-predicted $PM_{2.5}$ concentrations were
282 compared with site observations (Figure 8). NC was the most severely polluted area and the SP-EC model could capture the
283 $PM_{2.5}$ values and interannual differences. Particularly, the SP-EC model reproduce the sudden rebound of $PM_{2.5}$ pollution in
284 2018 (Figure 8e) that was mainly resulted from climate anomalies (Yin and Zhang 2020a).



285

286 **Figure 8: SP-EC predicted (shading) and site-observed (scatter) $PM_{2.5}$ concentrations (units: $\mu g/m^3$) in (a) 2014, (b) 2015, (c) 2016,**
287 **(d) 2017, (e) 2018 and (f) 2019. The boxes represent NC, the YRD and the PRD respectively.**

288 Due to the limitation of short sequence of data, recycling independent tests (RIT) were designed to further verify the
289 performance of the SP-EC model. In the RIT predictions, the prediction model was trained by samples from 2001 to the
290 expiration year of training data and the PM_{2.5} anomalies from the next year to 2019 were independently predicted. For
291 example, the prediction model trained by the data from 2001 to 2014 can produce independent predictions from 2015 to
292 2019. The expiration year of the training data moved forward from 2015 to 2019, so there were 15 independent predictions.
293 The PM_{2.5} concentration was independently predicted 5 times for 2019, 4 times for 2018, and so on. The PSS of PM_{2.5}
294 anomalies was 100%, not only relative to winters of 2001–2019 but also 2015–2019, indicating a high accuracy of prediction
295 in east of China. The predicted values for each year did not vary much (Figure 6d), indicating a high reliability and
296 robustness of the model. For example, when the SP-EC model was trained by the samples only from 2000 to 2014, the
297 predicted PM_{2.5} anomalies for 2018 and 2019 were also close to the results of leave-one-out validations and the
298 measurements.

299 **5 Conclusions and discussion**

300 The change of haze pollution consisted of long-term trend, interannual-decadal variations, synoptic disturbances and so
301 on. Seasonal prediction focused on predicting long-term trend and interannual-decadal variations 1~3 months in advance
302 (Wang et al., 2021). Because of the limitation of short observational period, many previous studies employed the number of
303 haze days as proxy of PM_{2.5} pollution to build statistical prediction model (Yin and Wang 2016; Yin et al., 2017; Dong et al.,
304 2021; Zhao et al., 2021; Chang et al., 2021). Since 2020, several high-resolution PM_{2.5} reanalysis datasets have been
305 successively released, which greatly increased the possibility for direct seasonal prediction of PM_{2.5} concentration that is
306 more familiar to decision makers and the public (Yin et al., 2021).

307 In this study, two seasonal prediction models were separately trained by emission factor (i.e., SP-SE) or preceding
308 climate predictors (i.e., SP-CV) to discuss their relative contributions. The SP-SE model could simulate the slow rising trend
309 of PM_{2.5} concentration before 2012 and the strong downward trend after 2012. However, it was incapable of importing the
310 interannual component. The SP-CV model benefited from the year-to-year increment approach and could introduce a large
311 portion of the linear trend except the sharp decrease of winter PM_{2.5} concentration from 2013. Furthermore, the SP-CV
312 model performed well in predicting the obvious interannual variation of PM_{2.5} concentration. We integrated the emission and
313 climate factors to establish the final prediction model (i.e., SP-EC), which could well reproduce both the trend and the
314 interannual variation of PM_{2.5} concentration. The area-averaged PSS was 81.4% in east of China and CC between observed
315 and predicted PM_{2.5} concentrations before (after) the detrending was 0.96 (0.74). The RMSEs were 6.8 in NC, 4.2 in the
316 YRD and 4.7 μg/m³ in the PRD, which were 44.3% (15.0%), 32.3% (12.5%) and 30.9% (9.6%) smaller than that the results
317 of SP-SE (SP-CV). Due to the implementation of the super-strict emission control measures, the air quality has been
318 substantially improved and this improvement was also perfectly predicted by the SP-EC model. During recycling
319 independent tests, the PSS of PM_{2.5} anomalies was 100%, demonstrating high accuracy and robustness. The high-resolution

320 PM_{2.5} prediction could provide scientific supports for air pollution control at the regional and city levels. For example, real-
321 time PM_{2.5} prediction is highly demanded for determining how to reduce anthropogenic emissions and how much should be
322 reduced; 10km×10km gridded PM_{2.5} information also had potentials to support finely and dynamically regional
323 managements and collaborations.

324 This study mainly focused on developments of seasonal PM_{2.5} prediction model. Related theories and methods are still
325 exploratory and need further discoveries. Although the SP-EC model was proved to be skilled, the underlying physical
326 mechanisms of climate predictors were not sufficiently explained and needed further in-deep studies. As shown in Figure 8f,
327 the SP-EC model failed to well predict the evident PM_{2.5} drops in east of China caused by COVID-19 quarantines in the
328 winter of 2019 (especially February in 2020) (Yin et al., 2021). Therefore, such sudden fluctuations of PM_{2.5} concentration
329 were not involved in the established prediction model. Furthermore, the EOF pattern of PM_{2.5} possibly changed under
330 climate change and must influence the climate component of PM_{2.5}, which should be updated in time. Although the SP-EC
331 model had high spatial resolution, it could only output winter-mean PM_{2.5} concentration. It was meaningful to build sub-
332 seasonal models to provide more detailed predictions. Modern weather and climate forecasts were heavily dependent on
333 numerical prediction models. Thus, it is imperative to design and develop numerical models that target at routine seasonal
334 prediction of air pollution (Yin et al., 2021).

335 **Data availability**

336 The monthly sea ice concentration and sea surface temperature (SST) dataset were provided by the Met Office Hadley
337 Centre: <https://www.metoffice.gov.uk/hadobs/hadisst/> (Rayner et al. 2003). Monthly soil moisture, snow depth, geopotential
338 height at 500hPa and 850hPa, sea level pressure and 10m wind were extracted from the fifth generation reanalysis product
339 (ERA5) produced by the European Center for Medium Range Weather Forecasts:
340 <https://cds.climate.copernicus.eu/#!/search?text=ERA5&type=dataset> (Hersbach et al. 2020). Annual emissions of ammonia,
341 nitrogen oxide, BOC, primary PM_{2.5}, and sulfur dioxide in China were derived from the MEIC model:
342 <http://www.meicmodel.org/> (Li et al., 2017). Hourly site-observed PM_{2.5} concentration during 2014–2019 were acquired
343 from the China National Environmental Monitoring Centre: <https://www.aqistudy.cn/historydata/> (CNEMC, 2021). The
344 long-term and high-resolution TAP PM_{2.5} concentration dataset during 2000-2019 can be downloaded from <http://tapdata.org>
345 (Geng et al. 2021b).

346 **Authors' contribution**

347 Wang H. J. and Yin Z. C. designed this research. Li Y. Y., Xu T. B. and Duan M. K. performed analyses and trained
348 prediction models. Yin Z. C. prepared the manuscript with contributions from all co-authors.

349 **Competing interests**

350 The authors declare no conflict of interest.

351 **Acknowledgements**

352 This research is supported by the National Natural Science Foundation of China (No. 42088101).

353 **References**

354 An, J., Chen, Y., Qu, Y., Chen, Q., Zhuang, B., Zhang, P., and Wu, Q.: An online-coupled unified air quality forecasting
355 model system, China, *Adv. Earth Sci.*, 33, 445–454, <https://doi.org/10.11867/j.issn.1001-8166.2018.05.0445>, 2018.

356 Chang, L., Wu, Z., and Xu, J.: Contribution of Northeastern Asian stratospheric warming to subseasonal prediction of the
357 early winter haze pollution in Sichuan Basin, China, *Sci Total Environ*, 751, 141823,
358 <https://doi.org/10.1016/j.scitotenv.2020.141823>, 2021.

359 Cheng, X. G., Boiyo, R., Zhao, T. L., Xu, X. D., Gong, S. L., Xie, X. N., and Shang, K.: Climate modulation of Niño3.4
360 SST-anomalies on air quality change in southern China: Application to seasonal forecast of haze pollution, *Atmos. Res.*, 225,
361 157–164, <https://doi.org/10.1016/j.atmosres.2019.04.002>, 2019.

362 Cohen, A. J., Brauer, M., Burnett, R., Anderson, H. R., Frostad, J., Estep, K., Balakrishnan, K., Brunekreef, B., Dandona, L.,
363 Dandona, R., Feigin, V., Freedman, G., Hubbell, B., Jobling, A., Kan, H., Knibbs, L., Liu, Y., Martin, R., Morawska, L.,
364 Pope, C. A., Shin, H., Straif, K., Shaddick, G., Thomas, M., van Dingenen, R., van Donkelaar, A., Vos, T., Murray, C. J. L.,
365 and Forouzanfar, M. H.: Estimates and 25-year trends of the global burden of disease attributable to ambient air pollution: an
366 analysis of data from the Global Burden of Diseases Study 2015, *The Lancet*, 389, 1907–1918,
367 [https://doi.org/10.1016/s0140-6736\(17\)30505-6](https://doi.org/10.1016/s0140-6736(17)30505-6), 2017.

368 Dong, Y., Yin, Z. C., and Duan, M. K.: Seasonal prediction of winter haze days in the Yangtze River Delta, China,
369 *Transactions of Atmospheric Sciences*, 44, 290–301, <https://doi.org/10.13878/j.cnki.dqkxxb.20200525001>, 2021.

370 Dun, M., Xu, Z., Wu, L., and Yang, Y.: Predict the particulate matter concentrations in 128 cities of China, *Air. Qual. Atmos.*
371 *Hlth.*, 13, 399-407, <https://doi.org/10.1007/s11869-020-00819-5>, 2020.

372 Gao, M., Sherman, P., Song, S., Yu, Y., Wu, Z., and McElroy, M. B.: Seasonal prediction of Indian wintertime aerosol
373 pollution using the ocean memory effect, *Science Advances*, 5, eaav4157, <https://doi.org/10.1126/sciadv.aav4157>, 2019.

374 Geng, G., Zheng, Y., Zhang, Q., Xue, T., Zhao, H., Tong, D., Zheng, B., Li, M., Liu, F., Hong, C., He, K., and Davis, S. J.:
375 Drivers of PM_{2.5} air pollution deaths in China 2002–2017, *Nat. Geosci.*, 14, 645-650, <https://doi.org/10.1038/s41561-021->

376 00792-3, 2021a.

377 Geng, G., Xiao, Q., Liu, S., Liu, X., Cheng, J., Zheng, Y., Xue, T., Tong, D., Zheng, B., Peng, Y., Huang, X., He, K., and
378 Zhang, Q.: Tracking Air Pollution in China: Near Real-Time PM_{2.5} Retrievals from Multisource Data Fusion, *Environ. Sci.*
379 *Technol.*, 55, <https://doi.org/12106-12115>, 10.1021/acs.est.1c01863, 2021b.

380 He, C., Liu, R., Wang, X. M., Liu, S. C., Zhou, T. J., and Liao, W. H.: How does El Nino-Southern Oscillation modulate the
381 interannual variability of winter haze days over eastern China?, *Sci. Total. Environ.*, 651, 1892–1902,
382 <https://doi.org/10.1016/j.scitotenv.2018.10.100>, 2019.

383 Hersbach, H., Bell, B., Berrisford, P., Hirahara, S., Horányi, A., Muñoz-Sabater, J., Nicolas, J., Peubey, C., Radu, R.,
384 Schepers, D., Simmons, A., Soci, C., Abdalla, S., Abellan, X., Balsamo, G., Bechtold, P., Biavati, G., Bidlot, J., Bonavita,
385 M., Chiara, G., Dahlgren, P., Dee, D., Diamantakis, M., Dragani, R., Flemming, J., Forbes, R., Fuentes, M., Geer, A.,
386 Haimberger, L., Healy, S., Hogan, R. J., Hólm, E., Janisková, M., Keeley, S., Laloyaux, P., Lopez, P., Lupu, C., Radnoti, G.,
387 Rosnay, P., Rozum, I., Vamborg, F., Villaume, S., and Thépaut, J. N.: The ERA5 global reanalysis, *Q. J. Roy. Meteor. Soc.*,
388 146, 1999-2049, <https://doi.org/10.1002/qj.3803>, 2020.

389 Hsu, P.-c., Zang, Y., Zhu, Z., and Li, T.: Subseasonal-to-seasonal(S2S) prediction using the spatial-temporal projection model
390 (STPM), *China, Transactions of Atmospheric Sciences*, 43, 212–224, <https://doi.org/10.13878/j.cnki.dqkxxb.20191028002>,
391 2020.

392 Huang, Y. Y., Wang, H. J., Zhang, P. Y.: A skillful method for precipitation prediction over eastern China, *Atmospheric and*
393 *Oceanic Science Letters*, 15 (1): 100133, <https://doi.org/10.1016/j.aosl.2021.100133>, 2022.

394 Li, M., Liu, H., Geng, G., Hong, C., Liu, F., Song, Y., Tong, D., Zheng, B., Cui, H., Man, H., Zhang, Q., and He, K.:
395 Anthropogenic emission inventories in China: a review, *Natl. Sci. Rev.*, 4, 834–866, <https://doi.org/10.1093/nsr/nwx150>,
396 2017.

397 Rayner, N. A., Parker, D. E., Horton, E. B., Folland, C. K., Alexander, L. V., Rowell, D. P., Kent, E. C., and Kaplan, A.:
398 Global analyses of sea surface temperature, sea ice, and night marine air temperature since the late nineteenth century. *J.*
399 *Geophys. Res.*, 108, 4407, <https://doi.org/10.1029/2002JD002670>, 2003.

400 Wang, H. J., Chen, H. P., and Liu, J. P.: Arctic sea ice decline intensified haze pollution in eastern China, *Atmospheric and*
401 *Oceanic Science Letters*, 8, 1–9, <https://doi.org/10.3878/AOSL20140081>, 2015.

402 Wang, H., Dai, Y., Yang, S., Li, T., Luo, J., Sun, B., Duan, M., Ma, J., Yin, Z., and Huang, Y.: Predicting climate anomalies:
403 A real challenge, *Atmospheric and Oceanic Science Letters*, <https://doi.org/100115>, 10.1016/j.aosl.2021.100115, 2021.

404 Wang, J. and Du, P.: Quarterly PM_{2.5} prediction using a novel seasonal grey model and its further application in health
405 effects and economic loss assessment: evidences from Shanghai and Tianjin, China, *Nat. Hazards*, 107, 889-909,

406 <https://doi.org/10.1007/s11069-021-04614-y>, 2021.

407 Wang, H., Sun, J., Lang, X.: Some New Results in the Research of the Interannual Climate Variability and Short-Term
408 Climate Prediction, China, Chinese Journal of Atmospheric Sciences, 32, 806–814, 2008.

409 World Health Organization: global air quality guidelines: particulate matter (PM_{2.5} and PM₁₀), ozone, nitrogen dioxide,
410 sulfur dioxide and carbon monoxide, <https://apps.who.int/iris/handle/10665/345329>, 2021.

411 Wu, J., Shi, Y., Asweto, C. O., Feng, L., Yang, X., Zhang, Y., Hu, H., Duan, J., and Sun, Z.: Fine particle matters induce
412 DNA damage and G2/M cell cycle arrest in human bronchial epithelial BEAS-2B cells, *Environ Sci Pollut Res Int*, 24,
413 25071-25081, <https://doi.org/10.1007/s11356-017-0090-3>, 2017.

414 Wu, L. F., Li, N., and Zhao, T.: Using the seasonal FGM(1,1) model to predict the air quality indicators in Xingtai and
415 Handan, *Environ Sci Pollut Res Int*, 26, 14683-14688, <https://doi.org/10.1007/s11356-019-04715-z>, 2019.

416 Xiao, Q., Zheng, Y., Geng, G., Chen, C., Huang, X., Che, H., Zhang, X., He, K., and Zhang, Q.: Separating emission and
417 meteorological contributions to long-term PM_{2.5} trends over eastern China during 2000–2018, *Atmos. Chem. Phys.*, 21,
418 9475-9496, <https://doi.org/10.5194/acp-21-9475-2021>, 2021.

419 Xiong, P., Yan, W., Wang, G., and Pei, L.: Grey extended prediction model based on IRLS and its application on smog
420 pollution, *Appl. Soft Comput.*, 80, 797-809, <https://doi.org/10.1016/j.asoc.2019.04.035>, 2019.

421 Xu, X., Zhao, T., Liu, F., Gong, S. L., Kristovich, D., Lu, C., Guo, Y., Cheng, X., Wang, Y., and Ding, G.: Climate
422 modulation of the Tibetan Plateau on haze in China, *Atmos. Chem. Phys.*, 16, 1365-1375, [https://doi.org/10.5194/acp-16-](https://doi.org/10.5194/acp-16-1365-2016)
423 1365-2016, 2016.

424 Yin, Z. C. and Wang, H. J.: Seasonal prediction of winter haze days in the north central North China Plain, *Atmos. Chem.*
425 *Phys.*, 16, 14843–14852, <https://doi.org/10.5194/acp-16-14843-2016>, 2016.

426 Yin, Z. C. and Wang, H. J.: Statistical Prediction of Winter Haze Days in the North China Plain Using the Generalized
427 Additive Model, *J. Appl. Meteorol. Clim.*, 56, 2411–2419, <https://doi.org/10.1175/jamc-d-17-0013.1>, 2017.

428 Yin, Z. C. and Wang, H. J.: The relationship between the subtropical Western Pacific SST and haze over North-Central North
429 China Plain, *Int. J. Climatol.*, 36, 3479-3491, <https://doi.org/10.1002/joc.4570>, 2016.

430 Yin, Z. C. and Wang, H. J.: The strengthening relationship between Eurasian snow cover and December haze days in central
431 North China after the mid-1990s, *Atmos. Chem. Phys.*, 18, 4753–4763, <https://doi.org/10.5194/acp-18-4753-2018>, 2018.

432 Yin, Z. C. and Zhang, Y. J.: Climate anomalies contributed to the rebound of PM_{2.5} in winter 2018 under intensified regional
433 air pollution preventions, *Sci Total Environ*, 726, 138514, <https://doi.org/10.1016/j.scitotenv.2020.138514>, 2020a.

434 Yin, Z. C., Li, Y. Y., and Wang, H. J.: Response of early winter haze in the North China Plain to autumn Beaufort sea ice,

435 Atmos. Chem. Phys., 19, 1439–1453, <https://doi.org/10.5194/acp-19-1439-2019>, 2019.

436 Yin, Z. C., Wang, H. J., Liao, H., Fan, K., and Zhou, B. T.: Seasonal to interannual prediction of air pollution in China:
437 Review and insight, *Atmospheric and Oceanic Science Letters*, 100131, <https://doi.org/10.1016/j.aosl.2021.100131>, 2022.

438 Yin, Z. C., Wang, H. J., and Guo, W. L.: Climatic change features of fog and haze in winter over North China and Huang-
439 Huai Area, China, *Sci. China Earth Sci.*, 58, 1370–1376, <https://doi.org/10.1007/s11430-015-5089-3>, 2015.

440 Yin, Z. C., Zhang, Y. J., Wang, H. J., and Li, Y. Y.: Evident PM_{2.5} drops in the east of China due to the COVID-19
441 quarantine measures in February, *Atmos. Chem. Phys.*, 21, 1581–1592, <https://doi.org/10.5194/acp-21-1581-2021>, 2021.

442 Yin, Z. C., Zhou, B. T., Chen, H. P., and Li, Y. Y.: Synergetic impacts of precursory climate drivers on interannual-decadal
443 variations in haze pollution in North China: A review, *Sci. Total Environ.*, 755, 143017,
444 <https://doi.org/10.1016/j.scitotenv.2020.143017>, 2020b.

445 Zhang, Q., Yin, Z. C., Xi, L., and co-authors.: Synergistic Roadmap of Carbon Neutrality and Clean Air for China 2021,
446 *Environmental Science and Ecotechnology*, Under Review, 2022.

447 Zhang, Q. and Geng, G. N.: Impact of clean air action on PM_{2.5} pollution in China, *Sci. China Earth Sci.*, 62, 1845–1846,
448 <https://doi.org/10.1007/s11430-019-9531-4>, 2020.

449 Zhao, Z., Liu, S. C., Liu, R., Zhang, Z., Li, Y., Mo, H., Wu, Y.: Contribution of climate/meteorology to winter haze pollution
450 in the Fenwei Plain, China, *Int. J. Climatol.*, 41, 4987-5002. <https://doi.org/10.1002/joc.7112>, 2021.

451 Zou, Y. F., Wang, Y. H., Zhang, Y. Z., and Koo, J.-H.: Arctic sea ice, Eurasia snow, and extreme winter haze in China,
452 *Science Advances*, 3, e1602751, <https://doi.org/10.1126/sciadv.1602751>, 2017.